Post-print of Meteorology and Atmospheric Physics, 135:8, https://doi.org/10.1007/s00703-022-00947-w

Quantifying the evolving role of intense precipitation runoff when calculating soil moisture trends in east Texas

Robert Kennedy Smith[1], Der-Chen Chang[1,2], José A. Guijarro[3], Yiming Chen[1]

1 Department of Mathematics and Statistics, Georgetown University, Washington, DC, USA

2 Graduate Institution of Business Admissions, College of Management, Fu Jen Catholic University, New Taipei City, Taiwan

3 State Meteorological Agency (AEMET), Balearic Islands Office, Palma, Spain

Abstract: Eastern Texas straddles a precipitation zone that transitions from semi-arid grasslands to the humid, rainy conditions of the northern Gulf Coast. While several studies have quantified the changing magnitude and frequency of daily extreme events, the paucity of hourly datasets have limited insight into how the growing proportion of rainfall exceeding hourly soil infiltration capacity has and will exacerbate the state's droughts. This paper builds on previous analysis, deploying algorithms with a temporal dimension to calculate soil moisture scarcity from evapotranspiration and precipitation data based on FAO-56 methodology and then introduces a daily estimate of the proportion of precipitation that flows off the ground surface rather than replenishing moisture deficits for soils with three different infiltrative capacities at 12 observation sites. The comparison of subsequent time series regression analyses showed that absorptive soils in east Texas have experienced modest, though mostly statistically insignificant, acceleration in drought trends after the incorporation of hourly rainfall intensity data: for the 24 soil samples (out of 36) with saturated hydraulic conductivity (K_{sat}) rates greater than 4.5 mm per hour, 14 had accelerated drying trends, five showed no change, and the remaining five displayed more gradual changes relative to their baseline trend magnitudes.

Keywords: Water stress, evapotranspiration, precipitation, soil moisture

1. Introduction

The largest state by area in the contiguous United States and the second-largest by total and urban population, Texas houses diverse climate zones and experiences frequent extreme precipitation events (Nielsen-Gammon et al. 2020a). Nearly 130 million acres of the state are farmland, with crops cultivated on approximately 23 percent of this total while the remaining lands are utilized for pasture and range (USDA 2017). As the state's population is projected to grow by over 70 percent in the next 50 years (Texas Water Development Board 2017), water usage and availability will become increasingly important to Texas' economic stability. Groundwater supplies continue to diminish from aquifer depletion, and the demand forecast, fueled by growth in municipal usage, shows an 87-percent increase over current consumption by 2070 (Texas Water Development Board 2017). The aforementioned forecast does not account for projected changes in drought severity from climate change (McGregor 2015; Nielsen-Gammon 2020a).

This analysis estimates trends in soil water scarcity over the eastern half of Texas from 1980 through 2020, where the majority of the population lives and most high-value crops are cultivated. Earlier calculations showed that under statistically insignificant annual precipitation trends, soil moisture scarcity, the cause of agricultural drought, increased in eastern Texas due to higher evapotranspiration rates (Smith and Chang 2020). Furthermore, sporadic rainfall coinciding with increasingly entrenched dry patterns leaves the region's agricultural fields and municipal water customers vulnerable to increasingly severe long-term, short-term, and flash droughts (Kloesel et al. 2018; Steiner et al. 2018). The finding agrees with climate model projections documenting decreases in soil moisture levels across the U.S., even in areas with stable or increasing annual precipitation, including the Southern Plains and Southeast (Seager et al. 2018; Trenberth et al. 2014; Ficklin et al. 2015). Nielsen-Gammon et al. (2020b) showed large projected increases in Texas' future soil moisture deficits that are anticipated to be especially acute during the summertime, a finding that can be buttressed by examining recent trends.

Warmer temperatures resulting from anthropogenic emissions have coincided with the increasing frequency and magnitude of extreme precipitation events across the U.S. and in the South (Melillo et al. 2014; Janseen et al. 2014; Skeeter et al. 2019). The Clausius-Clapeyron relationship estimates that for each degree celsius of warming, the atmosphere's moisture-holding capacity increases by approximately seven percent (Mishra et al. 2012). Moreover, average precipitable water values over the Gulf of Mexico have swelled by 7.3 percent from 1980 to 2018 (Wang et al. 2018). Recent precipitation trends have not been uniform by geographic region: the Northeast U.S. has experienced the most robust increases (Easterling et al. 2017; Janssen 2014). Eastern Texas straddles the more temperate, drier climate of the Southern Plains with the humid, wet climate of the Gulf Coast Region. Although this part of the state lacks orographically influenced microclimates, it is a transition zone from semi-arid prairies to the ubiquitous pine forests of the Southeast. Both the Southeast and Southern Plains have shown positive trends in the frequency and magnitude of heavy daily events, although to a lesser extent than the Northeast U.S. (Wuebbles et al. 2017). The trends are

projected to increase in the future due to changes in thermodynamic processes (Fischer 2015; Prein et al. 2015).

Precipitation in eastern Texas can largely be attributed to frontal air lifting during the cool season and convective air lifting during the warm season (Choi et al. 2008). Tropical cyclones are responsible for a significant yet sporadic portion of rainfall during the summer and fall seasons, reflected in elevated normal monthly values even though Houston receives precipitation every other year on average from such events (Trepanier and Tucker 2018). After 940 mm of rain flooded the city from Hurricane Harvey, recently published studies show a rise in extreme precipitation attributable to tropical cyclones in Southeast Texas (Zhang et al. 2018). Van Oldenborgh et al. (2017) estimated that global warming caused Hurricane Harvey's rains to fall 15 percent more intensely during the five-day period in August 2017 when the system stalled over the Houston area. Enhanced probabilities of these occurrences are caused by large-scale global circulation patterns (Bhatia et al. 2019) and local factors such as urban land-use change that can further destabilize the atmosphere (Zhang et al. 2018). Urbanization also impacts coastal precipitation not associated with cyclones by exacerbating the heat island effect and influencing the sea breeze (Burian and Shepherd 2005). Along with the aforementioned local circumstance, global factors may explain why coastal locations in Southeast Texas have generally seen more robust increases in extreme episodes relative to inland areas (Fagnant et al. 2020) since tropical cyclones making landfall have shown a positive correlation with time for larger accumulations of total event rains falling more heavily (Dhakal and Tharu 2018). In addition to amplifying the rate and duration at which precipitation falls, urban development leads to more severe flooding by increasing the amount of impervious surface cover (Sebastian et al. 2019).

Hourly precipitation data is limited due to the low number of observation locations that reliably measure at that timescale (Trenberth et al. 2017). Thus, a lower number of studies exist, and those that do draw from a limited pool of stations. Station data show that hourly winter precipitation rates in the U.S. South have shown the most robust increases relative to other seasons, a finding that is confirmed by regional studies (Mishra et al. 2012). Brown et al. (2019; 2020) have authored two analyses on precipitation in the Southeast, in which eastern Texas was included, showing broad increases in the hourly intensity rates, with divergent results at individual stations. Using a p value of 0.05, the authors found that 22 of 50 stations in 11 southern states showed statistically significant trends in average intensity, including a majority of their Texas sites. Although most stations in the sample did not show significant increases in the frequency of predetermined 90^{th}-percentile hourly events, Texas stations had the highest rates of annual growth – between 0.20% and 0.26% (Brown 2020). Interestingly, the authors did not find that the duration of dry spells was lengthening across the Southeast or in Texas. While this observation may appear to counter projections of increasing drought severity, agricultural drought depends on the balance between rainfall and evapotranspiration amounts, and therefore evapotranspiration may cause droughts to deepen more quickly even in periods with fewer dry days, as evident during flash droughts.

Seeking to answer how drying trends are not only impacted by precipitation amount and temporality, but also intensity, this analysis incorporates hourly rainfall data in soil water

balances. The calculation accounts for instances when the amount of water hitting the ground exceeds soil infiltration capacity and therefore runs off the surface rather than permeating it and supplying vegetation with moisture. Water scarcity trends in Texas with and without the hourly adjustments are presented. The comparison of trend direction and magnitude shows the increasing impact that heavy precipitation events have on drought conditions. As studies of deluges on soil moisture scarcity trends are sparse, this analysis determines if more frequent and larger episodes of extreme rainfall have accelerated dry conditions and to what extent, when applicable. Although these findings are state-specific, the use of publicly available datasets enables this analysis to be transferrable to any location or region with comprehensive, reliable climate observations

2. Materials and Methods

As extreme precipitation has become more frequent and heavier, a trend projected to continue, a greater amount of moisture that hits unsaturated soil surfaces would be expected to flow off rather than being absorbed and replenishing vegetative demand. The runoff becomes increasingly consequential as a greater percentage of precipitation exceeds the hourly soil infiltration rate. This section describes how hourly precipitation data, local soil infiltration capacities, and daily climate parameters at 12 locations were utilized by complementary algorithms to determine trends in eastern Texas soil moisture scarcity as measured by supplemental water demand. Figure 1 shows a summary flow chart of the forthcoming methods.

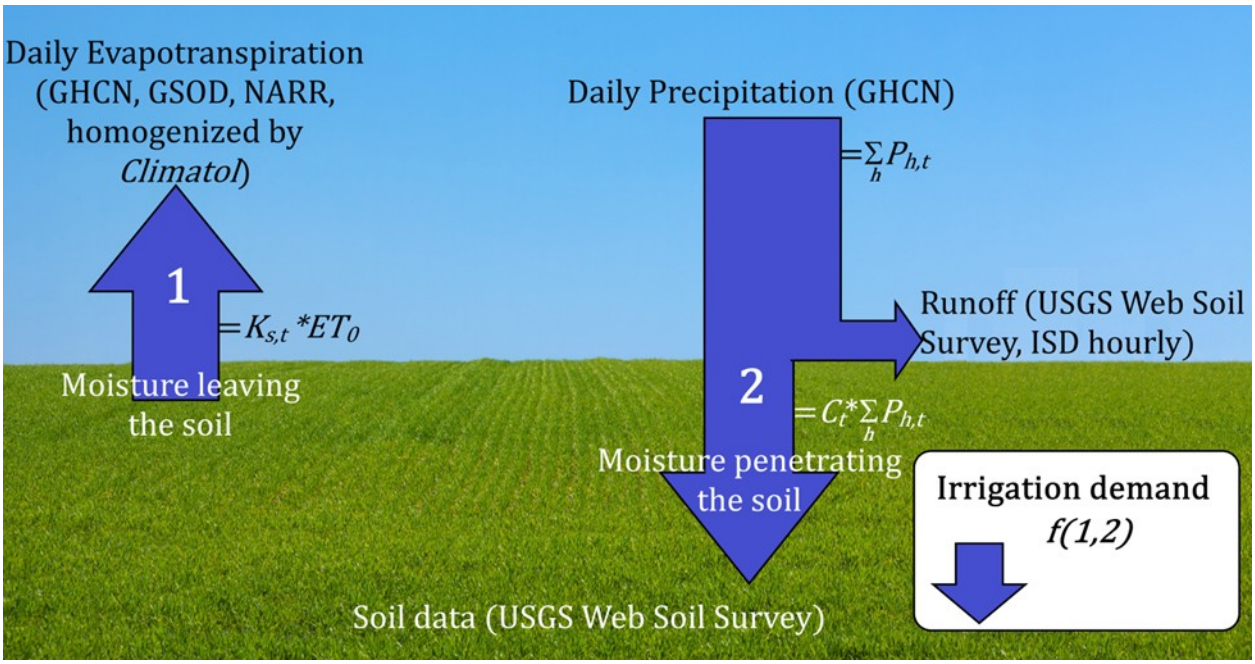

Fig. 1 Summary flow chart of the methodology, conducted for the 10th, 50th, and 90th-percentile soil classes at 12 locations, assuming the soils are below field capacity (arrows are not to scale and represent the flow of moisture relative to the ground surface).

2.1 Soil Moisture

Location-specific soil moisture levels in eastern Texas were determined by subtracting daily evapotranspiration rates, as calculated from the FAO-56 Penman-Monteith (PM) equation (Zontarelli et al. 2020), while adding daily precipitation reported by the Global Historical Climatology Network (GHCN), a highly accurate dataset maintained by the National Centers for Environmental Information (NCEI). The FOA-56 PM equation utilizes four climate parameters (humidity, temperature, wind, and solar radiation) as well as a latitude and elevation to calculate a simplified yet accurate representation of the determining physical and physiological components of the evapotranspiration process. Dewpoint temperature (needed for relative humidity), air temperature, and wind data were obtained from NCEI's Global Summary of the Day (GSOD) network. Solar radiation values are not tracked by the NCEI, so daily North American Regional Reanalysis (NARR) values were used (Mesinger et al. 2006). The assumed soil surface covering was well-watered, clipped, cool-season fescue grass 0.12 m in height (Wright 1993). An adjustment was made for days during which the average temperature remained below 4.5 °C and grass growth was stymied (Jensen and Allen 2020). Accurately calculating plot-specific ET_0 requires detailed land-use data and information on planting and harvesting cycles as well as crop growth, surface cover, wind resistance, and albedo. Therefore, a standard reference surface covering was chosen.

Reference evapotranspiration assumes unlimited water availability for optimal plant growth and is greater than evapotranspiration occurring when the vegetative covering has a constricted moisture supply during dry conditions. As fescue grass roots were assumed to penetrate the ground to a depth of one meter, the U.S. Department of Agriculture's Web Soil Survey (WSS) tool (USDA 2019) was consulted to determine the total available moisture capacity in the top one meter of soil. At the 12 locations (Figure 2), chosen by criteria explained later in this section, a 40,000-hectare plot (approximately 100,000 acres) was selected and the total available water (TAW) supply by soil type was obtained for the one-meter surface depth. Within the WSS database of soil types, each plot has a specific field capacity value (the total amount of water in mm the saturated plot holds) and a wilting point (the amount of water when moisture transfer is halted, also given in mm of moisture). The difference between the two values is each site's TAW. Under water-constricted conditions, evapotranspiration is equal to ET_0 until 40 percent of TAW, also known as the readily available water content (RAW), is depleted. At that point, a stress coefficient, $K_{s,t}$ (Equation 1) curtails the moisture transfer. If no water is introduced into the ground during this period, the value of $K_{s,t}$ reaches zero at the wilting point, with vegetation suffering irreparable damage at $K_{s,t}$ values below 0.2 (Wright 1993).

$$K_{s,t} = \frac{\mathrm{TAW}_t - \mathrm{ASMD}_{t-1}}{(1-0.4)\left(\mathrm{TAW}_t\right)} \text{for all} \, ASMD_{t-1} > RAW_{t-1} \qquad (1)$$

where $t = [1\ January\ 1979, \ldots, 31\ December\ 2020]$

$ASMD_{t-1}$ *represents the previous day's accumulated soil moisture deficiency.*

2.2 Station Selection Criteria and Data Homogenization

As the above calculations were paired with hourly precipitation data, NCEI's Integrated Surface Database (ISD) precipitation gauge network was examined for candidate stations having sufficient coverage. Within the eastern half of Texas and extreme northwest Louisiana, 12 ISD stations (Table 1, Figure 2) had greater than 95 percent coverage without showing a time-related bias; that is, when the number of missing records per year was regressed against its position in the analysis period timeline, none showed a statistically significant correlation. This was a perquisite for inclusion since hourly precipitation totals were matched with GHCN daily data, and incomplete ISD data would bias the extreme precipitation absorption curtailment multiplier calculations (to be described later in the section). Hourly values were extracted from raw ISD records and given Central Standard Time timestamps. A basic test for trends in average annual precipitation intensity was completed.

Table 1 Observation sites, East to West (GHCN, GSOD, and Integrated Surface Database (ISD) networks)

Station Name	Lat.	Long.	Station Name	Lat.	Long.
1. Shreveport Regional AP, LA	32.45	-93.82	7. Brownsville/SPI Int'l AP, TX	25.91	-97.42
2. Port Arthur/ SE TX Regional AP, TX	29.95	-94.02	8. Corpus Christi Int'l AP, TX	27.77	-97.51
3. Houston Intercontn'l Airport, TX	29.98	-95.36	9. San Antonio Int'l AP, TX	29.54	-98.48
4. Victoria Regional AP, TX	28.86	-96.93	10. Wichita Falls Muni. AP, TX	33.98	-98.49
5. DFW Int'l AP, TX	32.90	-97.02	11. Abilene Regional AP, TX	32.41	-99.68
6. Waco Regional AP, TX	31.62	-97.23	12. San Angelo Mathis Field, TX	31.35	-100.50

The 1979-2020 daily climate parameters imputed into the FOA-56 PM were homogenized by the *Climatol* algorithm (Guijarro 2019). It was not coincidental that all of the 12 stations with comprehensive ISD hourly coverage were located at large regional or international airports, also containing near-complete GHCN and GSOD series. To infill isolated missing daily observations, *Climatol* searched a cluster of the neighboring stations for the closest reporting value available. This closest value is not used directly, but as ratio to the mean of the series. After acquiring all records from the 12 GHCN and GSOD clusters, *Climatol* aggregated the daily data into monthly series and deployed the Standard Normal Homogeneity Test (SNHT), a procedure developed by Alexandersson in 1986 using a series of ratios that compare the observations of one measurement site with the cluster average to determine discontinuities within the aggregate means.

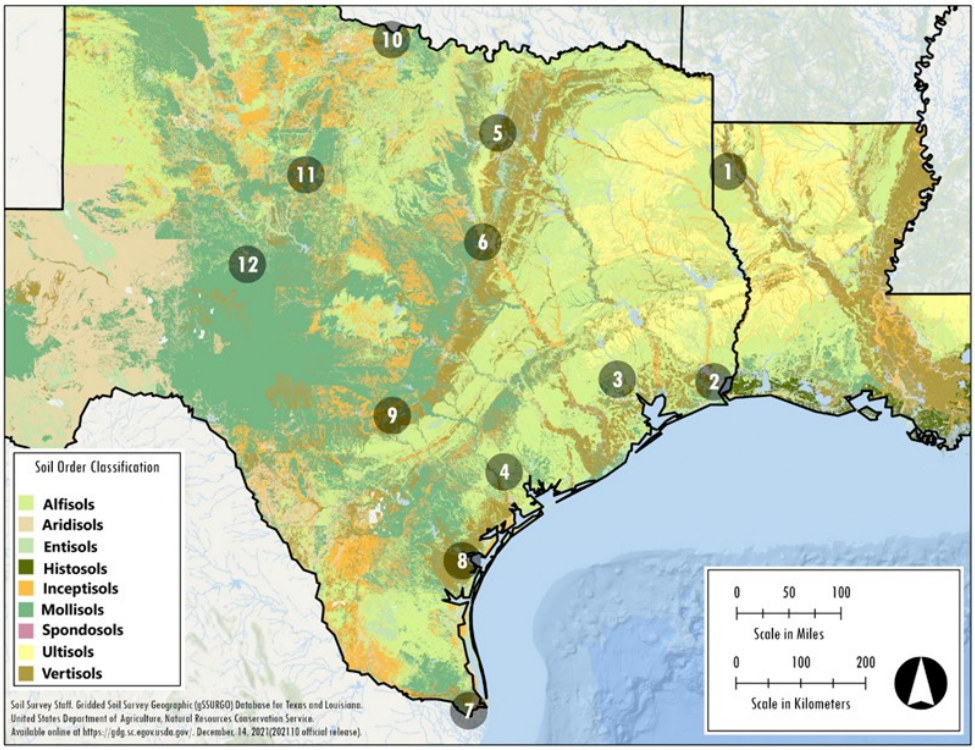

Fig. 2 Easternmost (1) to westernmost (12) observation sites, as referenced in all figures, with global soil classifications

Using an SNHT threshold of 25, *Climatol* identified breakpoints for each station, splitting the series at such occurrences. This is the default value of the algorithm, and while a bit conservative, has been established over the years to minimize the detection of false jumps in the average at the expense of missing jumps of minor importance (Guijarro 2021). The result was two or more partial subseries, that were reconstructed as multiple series to have a complete record throughout the 43-year period. The reconstruction mitigated potential bias from site-specific conditions and incomplete reporting histories by using normalized values with neighboring stations. The reader is referred to Smith et al. (2020) for a more comprehensive description of *Climatol*'s role in regional soil moisture analysis. Although this study utilized certified data, inhomogeneities arise when instruments are moved, replaced, or obstructed (Groisman and Legates 1994).

All reconstructed daily series were fed into the soil moisture algorithm (Figure 1), where daily $K_{s,t}$ values were calculated based on the proportion of the total available water supply that had been depleted. After 40 percent of the TAW had been exhausted, the evapotranspiration rate during subsequent days was given by $K_{s,t} * ET_0$. On days when precipitation fell or predetermined irrigation water amounts were added, depleted TAW was replenished until field capacity was reached, at which time the amount remaining was presumed to flow off the surface or percolate through the soil. This precludes rain that falls on saturated soils from augmenting soil moisture supply, but infiltration rates must be considered to determine the fraction of rainfall able to replenish TAW without running off.

2.3 Infiltration Rates and Hourly Runoff

Measuring infiltration rates across large areas is challenging due to inhomogeneous soils, and an explanation of the assumptions used in this analysis is provided in this subsection. Saturated hydraulic conductivity (K_{sat}) rates for the same Web Soil Survey (USDA 2020) plots from which TAW values were obtained and assumed to represent the maximum steady-state infiltration of each soil type. K_{sat} values cannot be averaged and varied widely across each plot: flat areas with sandy soils have steady-state infiltration rates exceeding 50 mm per hour whereas hilly terrain with clay soils often absorb less than 2.5 mm of moisture during the same timeframe. Areas unsuitable for the reference grass surface covering were excluded from the Web Soil Survey results, and K_{sat} values with corresponding TAW data from the remaining soil types were partitioned into 10th, 50th, and 90th-percentile values at each of the 12 climatological observation sites. These classifications represented the diversity of infiltration capacity within a relatively small distance and the uncertainties associated with the Web Soil Survey K_{sat} values and their representation of real-world infiltration. Displayed in Figure 2, eastern Texas soils are comprised of Alfisols, Inceptisols, Mollisols, Ultisols, and Vertisols (USDA 2020). While topographical variation plays a small role in infiltration capacity, soil consistencies are highly diverse, as can be seen in Table 2, which matches each percentile K_{sat}value to a corresponding Web Soil Survey description of a known soil type within each site's surrounding area of interest.

Web Soil Survey K_{sat} values originate from modified Uhland and O'Neal experimental results (USDA 2003; Uhland and O'Neal 1951), with topography considered. When a local soil survey is conducted, oftentimes less than once per decade, the majority soil type in each irregular subplot is represented. Approximately 10-30 unique K_{sat} subplot rates were reported for a 40,000-hectare site. This discretized mosaic is a simplified representation of the naturally blended soils. Moreover, observed K_{sat}values and the time during a wetting event at which they are observed are highly dependent on soil surface coverings (Rawls et al. 1993). Uhland and O'Neal's methodology measured the infiltration of water atop the soil and therefore did not account for runoff attributable to partial or complete crusting as heavy precipitation hits bare surfaces. This analysis assumed a grassy surface covering, which better approximated the experiments from which the Web Soil Survey values were obtained. Accurate infiltration curves for cultivated areas must consider the seasonality of crop cycles, tillage methods, and harvesting processes. Since such conditions can vary during different growing seasons, field K_{sat} observations are nontransferable (Rawls et al. 1982).

The second part of this discussion addresses the use of K_{sat} as the assumed infiltration rate when estimating the amount of heavy precipitation that is lost to runoff. For each day during the 1979-2020 analysis period, the proportion of daily precipitation that exceeded the 10th, 50th, and 90th-percentile K_{sat} values at the observation plots was quantified. The deployment of this rate in the analysis implicitly assumed a constant rainfall intensity over the one-hour time slice. Whenever the observed value was greater than the predetermined K_{sat} threshold, all remaining water hitting the ground within that hour was ineligible to replenish soil moisture deficits and was assumed to run off the surface as shown in Figure 1. For the curtailment factor, $C_{t,k}$, let $P_{h,t,k}$ equal the amount of precipitation falling in hour h on day t at

location k, obtained from the ISD network. Then for all $P_{h,t,k} > K_{sat}$, daily runoff, $Q_{h,t,k}$, is given by the following:

$$(2)\ Q_{h,t,k} = \sum_{h=1}^{24} P_{h,t,k} - K_{sat}$$

Table 2 USDA Web Soil Survey 10th, 50th and 90th infiltration percentile soil type descriptions

Stn.	10th-percentile Description	50th-percentile Description	90th-percentile Description
1	Wrightsville-Timpson complex, 0 to 1 percent slopes	Metcalf-Timpson complex, 0 to 2 percent slopes	Bowie fine sandy loam, 1 to 5 percent slopes
2	Franeau clay, 0 to 1 percent slopes, occasionally flooded	League clay, 0 to 1 percent slopes	Meaton-Levac complex, 0 to 1 percent slopes, rarely flooded
3	Cyfair-urban land complex, 0 to 1 percent slopes	Clodine-urban land complex, 0 to 1 percent slopes	Addicks loam, 0 to 1 percent slopes
4	Laewest-urban land complex, 0 to 3 percent slopes	Telferner fine sandy loam, 0 to 1 percent slopes	Inez fine sandy loam, 0 to 2 percent slopes
5	Ferris-urban land complex, 5 to 12 percent slopes	Crosstell fine sandy loam, 3 to 8 percent slopes	Gasil fine sandy loam, 3 to 8 percent slopes
6	Sanger clay, 1 to 3 percent slopes	Frio silty clay, 0 to 1 percent slopes, occasionally flooded	Chazos loamy fine sand, 1 to 3 percent slopes
7	Harlingen clay, 0 to 1 percent slopes	Sejita silty clay loam, 0 to 1 percent slopes, occasionally ponded	Rio Grande silt loam, 0 to 1 percent slopes
8	Aransas clay, 0 to 1 percent slopes, slightly saline, moderately sodic, frequently flooded	Aransas clay, 0 to 1 percent slopes, slightly saline, moderately sodic, frequently flooded	Orelia fine sandy loam, 0 to 1 percent slopes
9	Houston Black clay, 3 to 5 percent slopes	Austin silty clay, 2 to 5 percent slopes, moderately eroded	Whitewright clay loam 1 to 5 percent slopes
10	Mangum silty clay loam, 2 to 5 percent slopes	Winters loam, 1 to 3 percent slopes	Yomont very fine sandy loam, moist, 0 to 1 percent slopes, occasionally flooded
11	Tobosa clay, 0 to 1 percent slopes	Sagerton loam, 1 to 3 percent slopes	Clairemont silty clay loam, 0 to 1 percent slopes, occasionally flooded
12	Rioconcho and Spur soils, 1 to 5 percent slopes	Angelo clay loam, 0 to 1 percent slopes	Cho-Vernon complex, dry, 1 to 8 percent slopes

Then curtailment factor $C_{t,k}$ can be expressed by

$$(3)\ C_{t,k} = 1 - \frac{\sum_{h=1}^{24} Q_{h,t,k}}{\sum_{h=1}^{24} P_{h,t,k}}.$$

For days during which the K_{sat} threshold was not exceeded, $C_{t,k} = 1$, and the total amount of precipitation was available to recharge soil moisture as it was in the reference scenario, assuming the soil was below field capacity. Otherwise, the amount of water absorbed into the one-meter root zone was reduced by $C_{t,k}$.

Infiltration capacities as a function of time during events are often estimated by theory-based models developed by Green-Ampt (Nearing et al. 1993) and Philip (Bach et al. 1986). Such models deploy several parameters (effective suction, soil porosity, initial water content, etc.) when calculating how much moisture is absorbed by the soil. With time, maximum infiltration declines exponentially as the wetting front moves deeper into the subsurface, approaching a horizontal asymptote, K_{sat}, after several hours, once the surface layer becomes saturated. If an intense downpour falls on dry soil, ground infiltration capacity begins at high levels and rapidly declines within the first hour. Over the next several hours, the curve's slope approaches zero at K_{sat}. Use of K_{sat} therefore underestimated infiltration for downpours falling on dry soil and occurring at the beginning of wetting events. If heavy precipitation immediately followed previous rains, there would be minimal distance between the observed infiltration and the assumed K_{sat} rate.

2.4 Hypothetical Irrigative Water Demand

Moisture scarcity was represented by the amount of hypothetical irrigation water that was introduced to preserve the fescue grass in a healthy state: when $K_{s,t} \leq 0.7$ (Wright 1993), the algorithm introduced 25.4 m m (one inch) of moisture. For days that met this criterion when precipitation was reported, the irrigation amount was reduced by the amount of absorbed rain, unless daily adjusted rainfall exceeded 25.4 mm in which case no supplemental water was applied. The total amount of water was aggregated each month and an Autoregressive (AR) time series regression analysis was performed. The subsequent trends were calculated in R, with the AR order determined by the Akaike information criteria. With drought variability increasing, instances of heteroskedasticity were found during AR modeling. The Breusch-Pagan Test, which uses the Chi-Square test statistic on a subsequent regression of squared residuals, was deployed to all seasonally-adjusted regressions and when it showed a time-varying variance, a robust standard error procedure was completed that provided corrected significance levels of the regression coefficients. Statistical significance in this analysis was defined when $p \leq 0.1$.

2.5 Validation

The crux of the analysis lies in its ability to estimate soil moisture levels with a simplified methodology. Without adjusting for precipitation rates, the estimations performed better than an alternative, and improved accuracy was gained after incorporating intensity-induced runoff.

To demonstrate this, quality-controlled observed ground moisture values from NCEI's U.S. Climate Reference Network (USCRN) were obtained. The network measures water content directly from the subsurface rather than derived calculations from climate parameters (NOAA 2003). The data is highly accurate but sparse, as there are there only four Texas stations within the analysis area offering relatively complete observations: Austin, Bronte, Edinburg, and Palestine (Table 3). USCRN sites are also GHCN and GSOD stations, so daily climate observations were inputted into the soil moisture algorithm, with missing values again supplied by the closest GHCN or GSOD stations. Estimates from the algorithm were used to predict the USCRN observations. As a comparison, derived soil moisture values from the Climate Forecast System Reanalysis (CFSR) were also deployed as predictors for the same USCRN dataset. Both regressions covered a ten-year timeframe (2011-2020) due to the unavailability of earlier USCRN data. As columns 2 and 3 of Table 3 show, the uncurtailed algorithm estimates performed better than those of the CFSR, as measured by the R-squared degree of fit.

Table 3 R-squared values of 2011-2020 parameter-derived soil moisture estimates, relative to USCRN observations

USCRN Station	USCRN~CFSR, R-sq	USCRN~FAO-56, R-sq	USCRN~Adj. FAO-56, R-sq
Austin (30.62, -98.08)	0.69	0.72	0.74
Bronte (32.04, -100.24)	0.58	0.66	0.67
Edinburg (26.52, -98.06)	0.54	0.72	0.73
Palestine (31.77, -95.72)	0.69	0.59	0.59*

(*sandy soils at this location have a K_{sat} value that exceeded all 2011-2020 precipitation rates)

USCRN stations also record hourly precipitation, and intensities that exceeded the site-specific K_{sat} values as provided by NCEI were precluded from replenishing soil moisture deficits by reapplying a daily curtailment factor. Due to the high absorption rate of the soil beneath the Palestine station (91.5 percent sand), the adjustment was only applicable at three stations. While conclusions are limited from a modest improvement in capturing real-world conditions at three sites, accounting for intensity-induced runoff improved the algorithm's accuracy (Table 3, Column 4).

3. Results

Eastern Texas has become warmer, with all regions showing statistically-significant positive trends in average temperature from 1979 through 2020. Along with universal positive solar radiation trends, the warming has driven reference evapotranspiration rates higher at all 12 stations; five showed statistical significance (Stations 1, 5, 6, 9, 10). Precipitation trends were mixed, with five sites receiving more rainfall over the analysis period and seven recording less (Figure 3). As measured by ISD values, nine stations had positive intensity trends (annual precipitation divided by the number of hours during which it fell), although only one was statistically significant. A comparison of average 1979-2020 intensities and wetting hours are

presented in Figure 4. All subsequent figures display annual trends aggregated over the analysis period and do not represent historical values but rather initial and terminal expected normal conditions based on the calculated trends.

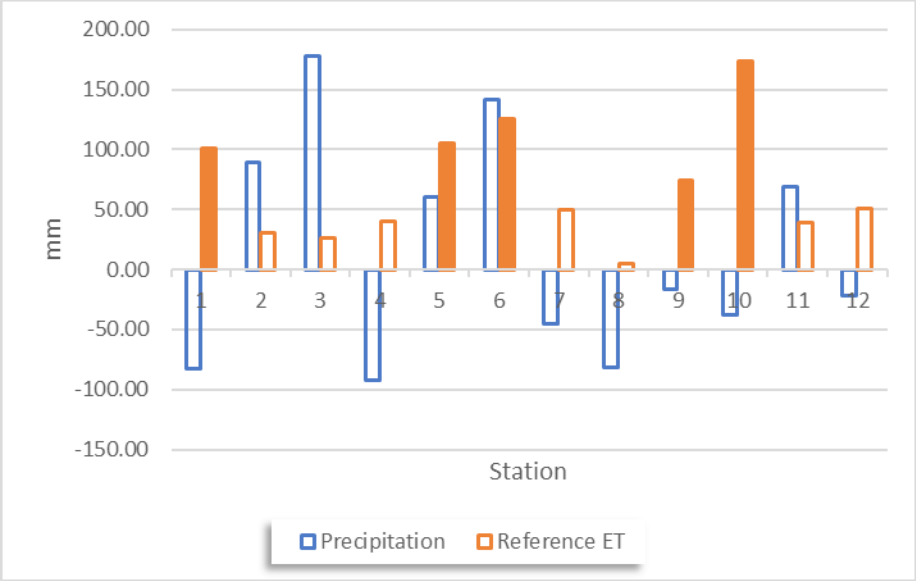

Fig. 3 Moving East to West, modeled 2020 average annual reference evapotranspiration and precipitation change, compared with modeled 1979 values (fill denotes statistical significance) (mm)

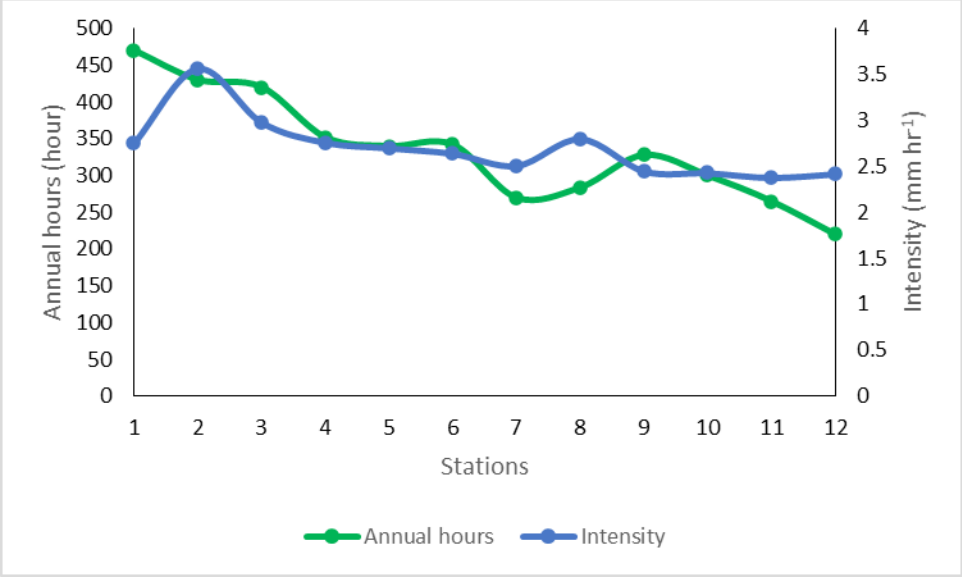

Fig. 4 Average 1979-2020 rainfall intensity (mm hr^{-1}) and average number of annual wet hours

The amount of water to preserve the reference surface grass in a well-watered state, a proxy for soil moisture scarcity, was calculated by the temporal balance between precipitation and evapotranspiration. With the first year of data (1979) omitted to subsequently calibrate root zone moisture levels, all observation sites showed positive trends from 1980-2020 (Figure 5). The increasing occurrence of aridity, even in regions where higher average amounts of precipitation are falling, was anticipated and agreed with earlier studies. Trends at five locations (1, 5, 6, 9, 10) were statistically significant. The findings were solely attributable to higher evaporative demand, as runoff had not yet been incorporated .

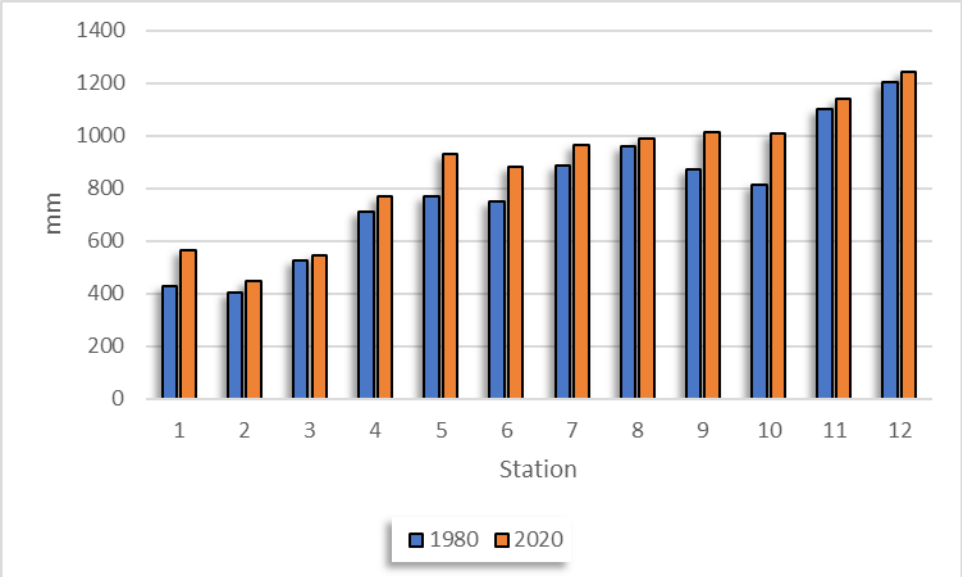

Fig. 5 AR modeled 2020 and 1980 average annual hypothetical vegetative water demand (mm)

Modeling runoff from extreme hourly precipitation events generally accelerated 1980-2020 drying trends, but the mixed results require interpretation. The amount of hourly accumulated precipitation that fell below the 10th, 50th, and 90th percentile K_{sat} thresholds are listed in Table 4, and vary widely based on the soil composition of each 40,000-hectare plot. In isolated instances, site infiltration rates at different percentiles were identical or similar if a specific soil type constituted a large proportion of the total. After the exclusion of unsuitable areas, such as quarries, muck pits, and sand, the 10th percentile soil classes were generally clays, transitioning to loam as the percentiles rose, with sandy and gravely soils comprising the 90th percentile classes, again shown in Table 2. Impacts on hypothetical irrigation time-series trends are shown in Figure 6 (modeled AR difference in expected irrigation demand at the end of the analysis period relative to the beginning), Figure 7 (the same information with only statistically significant trends displayed), and Figure 8 (the 1980-2020 expected difference when compared to the uncurtailed infiltration data over the identical timeframe). For 10th percentile K_{sat} values, six of 12 stations showed decreases in the rate of drying relative to unrestricted hourly infiltration. The five stations with statistically significant 1980-2020 growth in water demand,

Stations 1, 5, 6, 9, and 10, retained their significance. Using 50th percentile infiltration rates, eight of 12 stations had accelerated drying, with two additional sites, Station 2 and 4, having a significant, positive trend. Finally, with 90th percentile soil class infiltration capacities, all seven stations with different trends from the unrestricted scenario showed increases in soil moisture deficits (Figures 7 and 8). As Table 4 illustrates, 90th percentile K_{sat} values for the remaining five locations are so high that these soils absorbed more than 99.5 percent of total 1979-2020 accumulated precipitation. The negligible to nonexistent extreme episodes that exceeded the thresholds were not sufficient to cause a measurable impact on trends. Although none of the 12 locations showed a decrease in the rate of drying relative to the reference scenario for this percentile, differences in the magnitude of change are expectedly small due to the rarity of such intense deluges.

Table 4 Percentage of 1979-2020 precipitation eligible to recharge soil moisture levels by K_{sat} percentile value

Station / percentile	10th	50th	90th	Station / percentile	10th	50th	90th
1. Shreveport Regional AP	75.5%	94.7%	99.9%	7. Brownsville/SPI Int'l AP	26.9%	81.4%	100.0 %
2. P. Arthur/ SE TX Reg. AP	20.1%	20.8%	87.2%	8. Corpus Christi Int'l AP	45.8%	45.8%	80.2%
3. Houston Intercontn'l AP	76.9%	90.1%	98.6%	9. San Antonio Int'l AP	27.0%	52.7%	98.2%
4. Victoria Regional AP	24.6%	63.8%	99.7%	10. Wich. Falls Muni. AP	56.0%	94.0%	99.4%
5. DFW Int'l AP	26.9%	73.0%	100.0%	11. Abilene Regional AP	30.4%	97.3%	99.0%
6. Waco Regional AP	26.9%	86.1%	99.6%	12. S. Angelo Mathis Field	29.6%	93.9%	99.5%

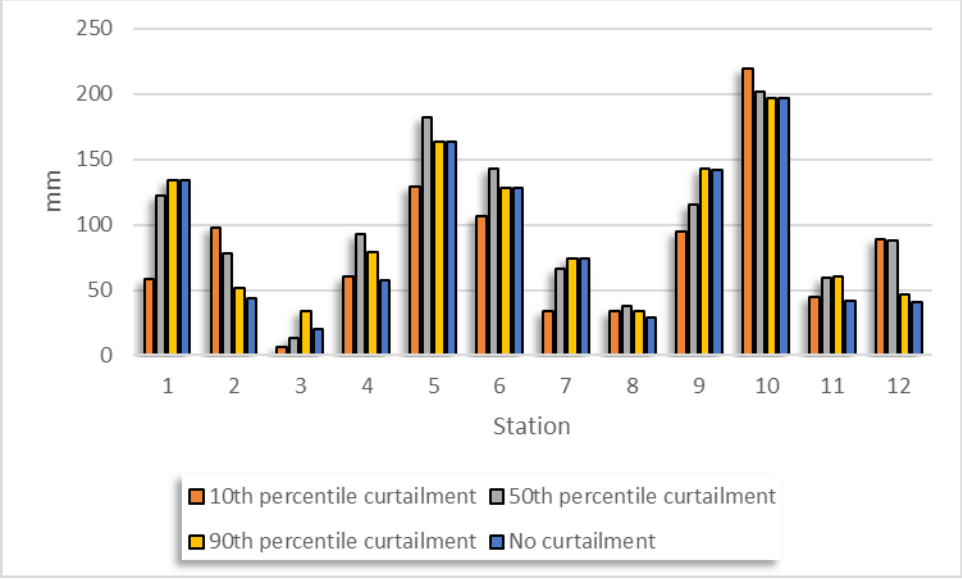

Fig. 6 Comparisons of AR modeled 1980-2020 change in hypothetical irrigative water demand by soil infiltration rate) percentile (mm)

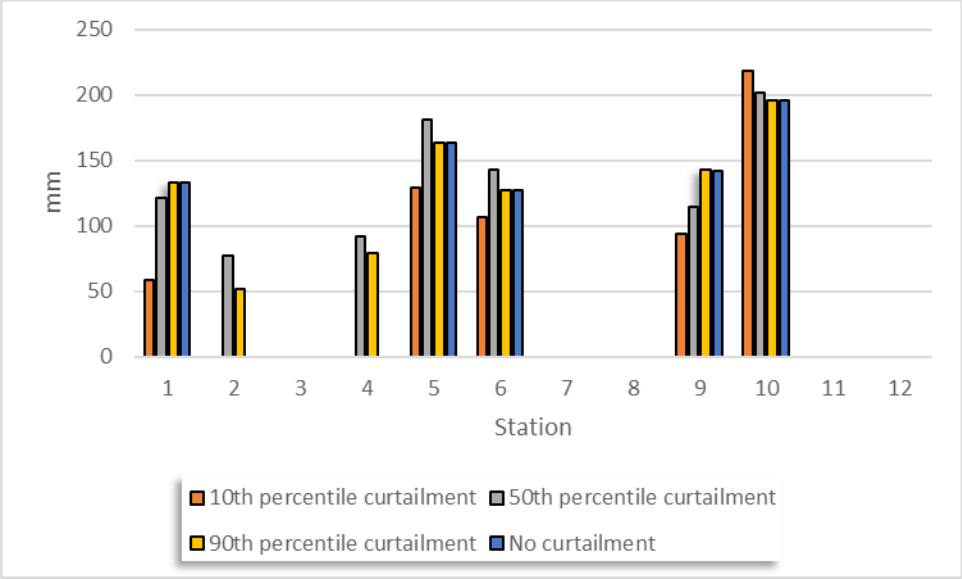

Fig. 7 Statistically significant comparisons of AR modeled 1980-2020 change in hypothetical irrigative water demand by soil infiltration rate) percentile (mm)

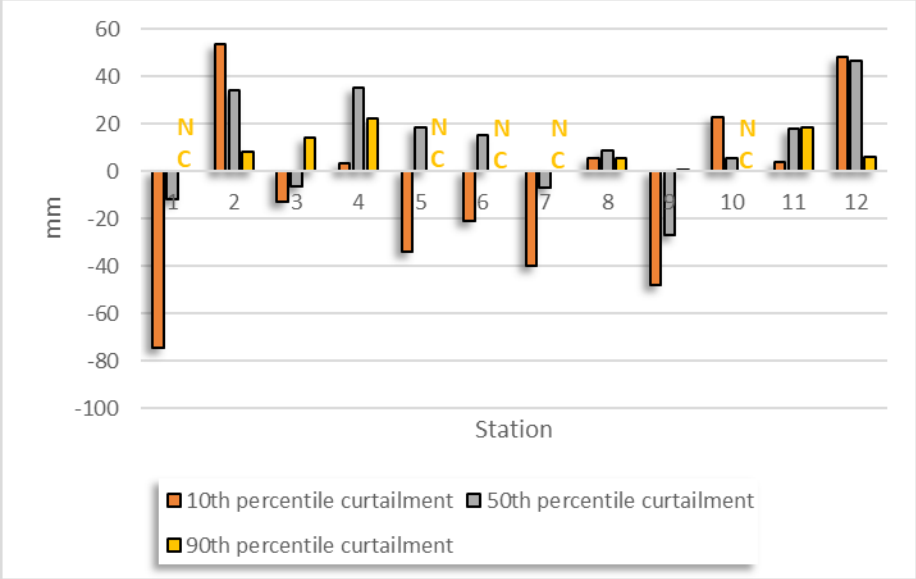

Fig. 8 10th, 50th, and 90th K_{sat} percentile 1980-2020 change in hypothetical irrigative water demand, relative to unrestricted infiltration (with $\frac{N}{C}$ signifying no change)

4. Discussion

4.1 Interpretation of Results

Upon first inspection, the mixed results in Figure 8 relative to the unrestricted hourly absorption baseline may appear to suggest that increases in extreme precipitation have not exacerbated soil dryness. In fact, different soil classes were affected in unique ways by the

increased frequency and magnitude of heavy downpours. Since the observation sites in east Texas have not shown consistent trends in accumulated precipitation, augmented intensities equated to fewer hours of recorded rain: AR modeling of the number of precipitation hours showed declines at 11 of 12 stations, although none was statistically significant. The absorptive capacity of clay soils represented by the station-specific 10th percentiles are low – in some cases approximately one mm hour^{-1}— so the majority of light and moderate rainfall flows off the surface (Wilcox et al. 2007). As the number of hours during which rain fell declined, there were fewer such occurrences. With stable precipitation amounts, this decrease would be counteracted by heavier events, however low infiltration rates already preclude all but a small proportion from penetrating the ground surface. Neither of the opposing factors was dominant at the observation sites, as shown by the even divide in accelerated drying among 10th percentile soil classes.

For more porous soils, runoff potential from intense downpours was more consequential than the curtailment in the number of events. The higher absorption rates of these 50th and 90th percentile soil classes equated to less frequent runoff occurrences throughout the analysis period, so the increased volume from individual episodes grew in importance. It is also noted that three of the four stations with decelerating 50th percentile trends relative to the baseline had negative precipitation trends with respect to time, further curtailing runoff opportunities. At the 90th percentile, the capacity of sandy soils to absorb all but the most extreme episodes diminished the magnitude of trend acceleration, as there were smaller differences with the unbounded reference case, but added clarity with respect to the positive trend signals at all locations that showed change.

This interpretation is summarized in Figure 9: a scatterplot that displays the results differently from the previous figures. Its x-axis, average annual precipitation, spatially differentiates the 12 stations. The y-axis, measuring K_{sat}, was truncated above 50 mm per hour: stations with 90th percentile infiltration rates exceeding that value are shown at the top of the plot. There are therefore 36 dots representing the 10th, 50th, and 90th infiltration percentiles for the 12 stations, although when a station's K_{sat} values were similar at different percentiles, the dots cannot be visually distinguished. The color of each dot is determined by the change in hypothetical irrigative water demand, as shown in Figure 8. No change is represented by a colorless dot. A positive (negative) change in demand is represented by blue (red) fill – the greater the magnitude of change, the deeper the shade of color. For example, the wettest and driest stations, #2 and #12, respectively, had increased demand for all three percentile classes . This is represented by positive bars in Figure 8 and blue dots at the left and righthand ends of the scatterplot (Figure 9). Shreveport (Station 1), the second-wettest location, had the largest overall drop in irrigative demand for its 10th percentile soils, shown by the negative bar in Figure 8 and as the deep-red dot located at the coordinates (1301, 12) in Figure 9. As the Figure reveals, absorptive soils, regardless of their respective percentiles, did not experience large irrigative demand reductions – notwithstanding the singular aforementioned exception at Shreveport: five of the six largest demand reductions were seen in soils with K_{sat} values below 4.5 mm per hour.

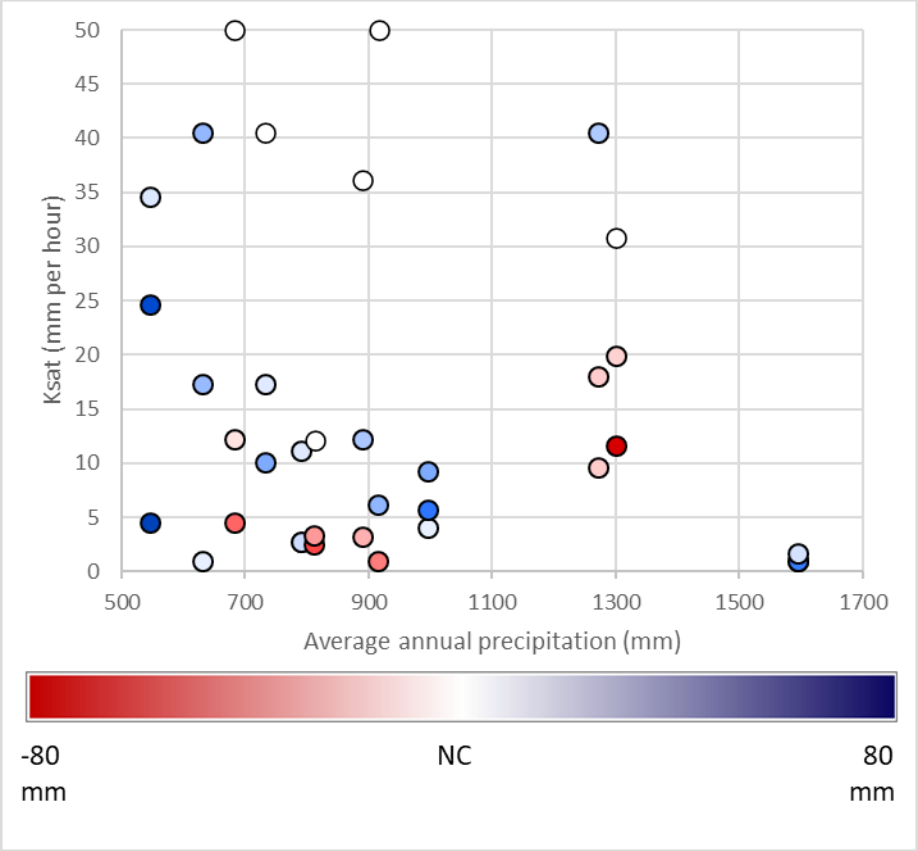

Fig. 9 Scatterplot of the 10th, 50th, and 90th K_{sat} percentile 1980-2020 change in hypothetical irrigative water demand: blue denotes positive change, red denotes negative change.

4.2 Limitations of the Analysis

While it is an important distinction for water supply security and flood mitigation planning whether the moisture hitting the ground percolates through saturated soils or exceeds the infiltration rate and flows off the surface, this algorithm represented both events under the same classification: ineligible to recharge moisture in the vegetative root zone. High-quality gridded data products available for use in daily, weekly, or monthly trend analysis are not available for hourly precipitation over a four-decade period. More recent high-resolution products exist using analyzed historical radar data, such as the NEXRAD Level III sets, but the earliest sites began reporting in the early 1990s, and many did not come online until the middle or later portion of that decade (NOAA 2020). The reconstructed GHCN, GSOD, and ISD hourly sets utilized in this analysis are highly reliable and have a 43-year period of continuous reporting, but resulted in a small sample.

In addition to the low number of climatological reporting stations, uncertainties and complexities associated with infiltration rate calculations also posed difficulties when relating the analysis to real-world conditions. Real-time infiltration is a function of initial soil moisture, and the daily algorithm could not capture precise conditions at the start of each event. There are also soil behaviors that the Uhland and O'Neal methodology did not capture such as the

absorption-impeding surface crust that forms during heavy episodes. Highly-impenetrable clay soils are prone to deep cracking, providing enhanced but variable infiltration opportunities that are not easily replicated in laboratory experiments (Rawls and Brakensiek 1989; Matlack et al. 1989; Bronswijk 1987). For the 40,000-hectare plots, percentiles were used to communicate ranges of uncertainty. Determining the average infiltration rate for the 12 areas of interest is appropriate due to the factors discussed earlier, but the absence of a single number can be unsatisfying when it precludes sweeping characterizations and succinct conclusions. For stakeholders, average calculations can present challenges based on their interpretations: an urban planner may find mean values useful for water management, while a farmer cultivating vegetation on clay soils may be misled by a singular number. As noted, the infiltration rate can vary by several orders of magnitude based on the seasonality of crop cover, tilling methodology, and harvesting cycle, while soil composition remains constant (Dabney 1998).

5. Conclusion

Eastern Texas has become more arid over the past four decades even though annual expected precipitation has not declined. Higher temperatures have enhanced reference evapotranspiration, and together with the timing of rainfall events, soil moisture deficits have deepened.

As each soil class responds differently to more precipitation falling during fewer hours, the impacts varied. For loamy and sandy soils in the 50th and 90th percentiles, consideration of hourly runoff resulted in accelerated drying for 15 of the 19 cases that had different trends relative to the unconstrained assumptions (Figure 8). Even though the accelerated drying was modest and only statistically significant in once instance, the analysis opened several avenues of further investigation. Especially in wetter areas that are vulnerable to water supply insecurity and have high demand from municipal and agricultural usage, the increasing proportion of extreme precipitation that does not replenish soil moisture and instead runs off should be factored into projections that quantify the growing risk of drought in spite of stable or rising average annual precipitation. As much of Eastern Texas is a low-lying area reliant on bayou drainage systems, future infrastructure projects should also account for the higher amounts of runoff water expected in the future if current trends continue.

Data Availability Statement:

All climate data (Global Historical Climatology Network, Global Summary of the Day, Integrated Surface Database, and U.S. Climate Reference Network) is publicly available and was obtained from the National Centers for Environmental Information (https://gis.ncdc.noaa.gov/maps/ncei, https://www.ncdc.noaa.gov/crn), with the exception of solar radiation data, publicly available at http://climateengine.org.

References

Bach, L., Wierenga, P., and Ward, T. (1986) Estimation of the Philip Infiltration Parameters from Rainfall Simulation Data. *Soil Sci. Soc. Am. J.* **50**, 1319-1323.

Bhatia, N., Singh, V., Lee, K. (2019) Variability of extreme precipitation over Texas and its relation with climatic cycles. *Theor. Appl. Climatol.*, **138**, 449-467.

Bronswijk, J. (1987) Modeling of water balance, cracking and subsidence of clay soils. *J. Hydrol.*, **97**. 199-212.

Brown, V., Keim, B., and Black, A. (2019) Climatology and Trends in Hourly Precipitation for the Southeast United States. *J. Hydrometeorol.*, **20**, 1737-1755.

Brown, V., Keim, B., and Black, A. (2020) Trend Analysis of Multiple Extreme Hourly Precipitation Time Series in the Southeastern United States. *J. Climate Appl. Meteor.*, **59**, 427-442.

Burian, S. and Shepherd, J., (2005) Effect of urbanization on the diurnal rainfall pattern in Houston. *Hydrol. Process.*, **19** (5), 1089-1103.

Choi, J., Socolofsky, S., Olivera, F. (2008) Hourly Disaggregation of Daily Rainfall in Texas Using Measured Hourly Precipitation at Other Locations. *J. Hydrol. Eng.*, **13** (6).

Dabney, S. (1998) Cover crop impacts on watershed hydrology. *J. Soil Water Conserv*, **53**. 207-213.

Dhakal N, Tharu B (2018) Spatio-temporal trends in daily precipitation extremes and their connection with North Atlantic tropical cyclones for the southeastern United States. Int. J. Climatol., **38** (10), 3822-3831.

Easterling, D., Kunkel, K., Arnold, J., Knutson, T., LeGrande, A., Leung, L., Vose, R., Waliser, D., and Wehner, M. (2017) Precipitation change in the United States. In *Climate Science Special Report: Fourth National Climate Assessment*, *Volume I*. [Wuebbles, D., Fahey, D., Hibbard, K., Dokken, D., Stewart, B., and Maycock, T. (eds.)]. U.S. Global Change Research Program, Washington, DC, USA 207-230. doi:10.7930/J0H993CC.

Fagnant, C., Gori, A., Sebastian, A., Bedient, P., and Ensor, K. (2020) Characterizing spatiotemporal trends in extreme precipitation in Southeast Texas. *Nat. Hazards*, **104**, 1597-1621.

Ficklin, D., Maxwell, J., Letsinger, S., Gholizadeh, H. (2015) A Climate deconstruction of recent drought trends in the United States. *Environ. Res. Lett.*, **10** (4).

Fischer, E., and Knutti, R. (2015) Anthropogenic contribution to global occurrence of heavy-precipitation and high-temperature extremes. *Nat. Climate Change*, **5**, 560-564.

Groisman, P. and Legates, D. (1994) The accuracy of the United States precipitation data. *Bull. Amer. Meteor. Soc.*, **75**, 215-227.

Guijarro, J. (2019) Package *Climatol. https://CRAN.R-project.org/package=climatol* . Accessed 25 November 2022.

Guijarro, J. (2021) Homogenization of climatic series with Climatol. *https;//climatol.eu/homog_climatol-en.pdf*. Accessed 25 November 2022.

Janssen, E., Wuebbles, D., Kunkel, K., Olsen, S., and Goodman, A. (2014) Observational and model-based trends and projections of extreme precipitation over the contiguous United States. *Earth's Future*, **2**, 99-113.

Jensen, M. and Allen, R. (2016) *Evaporation, Evapotranspiration, and Irrigation Water Requirements*. 2nd ed. ASCE, https://ascelibrary.org/doi/book/10.1061/9780784414057. Accessed 1 November 2020.

Kloesel, K., Bartush, B., Banner, J., Brown, D., Lemery, J., Lin, X., Loeffler, C., McManus, G., Mullens, E., Nielsen-Gammon, J., Shafer, M., Sorensen, C., Sperry, S., Wildcat, D., and Ziolkowska, J. (2018) Southern Great Plains. In *Impacts, Risks, and Adaptation in the United States: Fourth National Climate Assessment, Volume II* [Reidmiller, D., C.W. Avery, C., D.R. Easterling, D., K.E. Kunkel, K., K.L.M. Lewis, K., T.K. Maycock, T., and B.C. Stewart, B. (eds.)]. U.S. Global Change Research Program, Washington, DC, USA, pp. 987–1035. doi: 10.7930/NCA4.2018.CH23.

Matlack, K. S., Houseknecht, D., and Applin, K. (1989) Emplacement of clay into sand by infiltration. *J. Sediment. Res.*, **59**. 77-87.

McGregor, K., 2015: Comparison of the Recent Drought in Texas to the Drought of Record Using Reanalysis Modeling. *Papers in Appl. Geogr.*, **1**, 34-42.

Melillo, J., Richmond, T., and Yohe, G., Eds. (2014) Climate Change Impacts in the United States: The Third National Climate Assessment. U.S. Global Change Research Program, 841 pp. doi:10.7930/J0Z31WJ2.

Mesinger, F., DiMego, G., Kalnay, E., Mitchell, K., Shafran, P., Ebisuzaki, W., Jovic, D., Woollen, J., Rogers, E., Berbery, E., et al. (2006) North American Regional Reanalysis. *Bull. Amer. Meteor. Soc.*, **87**, 343-360.

Mishra, V., Wallace, J., Lettenmaier, D., (2012) Relationship between hourly extreme precipitation and local air temperature in the United States. *Geophys. Res. Lett.*, **39**, L16403.

National Oceanic and Atmospheric Administration (2003) *United States Climate Reference Network (USCRN) Program Development Plan*. United States Department of Commerce, Washington, DC, USA.

National Oceanic and Atmospheric Administration, National Centers for Environmental Information (2020). NOAA Next Generation Radar (NEXRAD) Level 3 Products, available online: https://www.ncei.noaa.gov/access/metadata/landing-page/bin/iso?id=gov.noaa.ncdc:C00708. Accessed 12 December 2020.

Nearing, M., Liu, B., Risse, L., Zhang, X. (1993) Curve Numbers and Green-Ampt Effective Hydraulic Conductivities. *Water Resour. Bull.*, **32**, 125-136.

Nielsen-Gammon, J., Escobedo, J., Ott, C., Dedrick, J., and Van Fleet, A. (2020a) Assessment of Historic and Future Trends of Extreme Weather in Texas, 1900-2036. Texas A&M University, Office of the Texas State Climatologist., 40 pp.

Nielsen-Gammon, J., Banner, J., Cook, B., Tremaine, D., Wong, C., et al. (2020b) Unprecedented Drought Challenges for Texas Water Resources in a Changing Climate: What Do Researchers and Stakeholders Need to Know? *Earth's Future*, **8**, e2020EF001552.

Prein, A., Rassmussen, R., Ikeda, K., Liu, C., Clark, M., and Holland, G. (2015) The future intensification of hourly precipitation extremes. *Nat. Climate Change*, **7**, 48-52.

Rawls, W., D. Brakensiek, and K. Saxton (1982) Estimation of Soil Water Properties. *Transactions of the ASAE*. The American Society of Agricultural Engineers. Paper No. 81-2510

Rawls, W., Ahuja, L., Brakensiek, D., and Shirmohammadi, A. (1993) Infiltration and Soil Water Movement. In *Handbook of Hydrology* [Maidment, D (ed.)]. McGraw-Hill, Inc., New York, NY, USA. ISBN: 0070397325.

Rawls, W.J., Brakensiek, D.L. (1989). Estimation of Soil Water Retention and Hydraulic Properties. In: Morel-Seytoux, H.J. (eds) *Unsaturated Flow in Hydrologic Modeling*. NATO ASI Series, vol 275. Springer.

Seager, R., Lis, N., Feldman, J., Ting, M., Williams, A., Nakamura, J., Liu, H., and Henderson, N. (2018) Whither the 100th Meridian? The Once and Future Physical and Human Geography of America's Arid-Humid Divide. Part I: The Story so Far. *Earth Interactions*, **22**, 1-22.

Sebastian, A., Gori, A., Blessing, R., van der Wiel, K., Bass, B. (2019) Disentangling the impacts of human and environmental change on catchment response during Hurricane Harvey. *Environ. Res. Lett.*, **14**, 124023.

Skeeter, W., Senkbeil, J., and Keellings, D. (2019) Spatial and temporal changes in the frequency and magnitude of intense precipitation in the southeastern United States. *Int. J. Climatol.*, **39**, 768-782.

Smith R, Chang D (2020) Utilizing recent climate data in eastern Texas to calculate trends in measures of aridity and estimate changes in watering demand for landscape preservation. *J. Clim. Appl. Meteor.*, **59**:143–152

Smith, R., Guijarro, J, and Chang, D. (2020) Utilizing homogenized observation records and reconstructed time series data to estimate recent trends in Mid-Atlantic soil moisture scarcity. *Theor Appl Climatol*. https://doi.org/10.1007/s00704-020-03467-y

Steiner, J., Briske, D., Brown, D., Rottler, C. (2018) Vulnerability of Southern Plains agriculture to climate change. *Climatic Change*, **146**, 201-218.

Texas Water Development Board (2017) *State Water Plan*. State of Texas, 134 pp.

Trenberth, K., Dai, A., van der Schrier, G., Jones, P., Barichivich, J., Briffa, K., and Sheffield, J. (2014) Global warming and changes in drought. *Nature Climate Change*, **4**, 17-22.

Trenberth, K., Zhang, Y., and Gehne, M. (2017) Intermittency in precipitation: Duration, frequency, intensity, and amounts using hourly data. *J. Hydrometeor.*, **18**, 1393-1412.

Trepanier, J., and Tucker, C. (2018) Event-Based Climatology of Tropical Cyclone Rainfall in Houston, Texas and Miami, Florida. *Atmosphere*, **9**.

Uhland, R. and O'Neal, A. (1951) *Soil permeability determination for use in soil and water conservation*. *SCS-TP-101*. United States Department of Agriculture, Soil Conservation Service, Washington, DC, USA.

United States Department of Agriculture, National Resources Conservation Service (2003) *Soil Survey Technical Note 6: Saturated Hydraulic Conductivity: Water Movement Concepts and Class History*, Washington, DC, USA.

United States Department of Agriculture, Economic Research Service (2017) Major Land Uses. https://www.ers.usda.gov/data-products/major-land-uses. Accessed 20 November 2020.

United States Department of Agriculture, National Resources Conservation Service (2019) Web Soil Survey. https://websoilsurvey.sc.egov.usda.gov. Accessed 17 December 2020.

van Oldenborgh, G., van der Wiel, K., Sebastian, A., Singh, R., Arrighi, J., Otto, F., Haustein, K., Li, S., Vecchi, G., and Cullen, H. (2017) Attribution of extreme rainfall from Hurricane Harvey, August 2017. *Environ. Res. Lett.*, **12** (12).

Wang, S., Zhao, L., Yoon, J., Klotzbach, P., Gillies., R. (2018) Quantitative attribution of climate effects on Hurricane Harvey's extreme rainfall in Texas. *Environ. Res. Lett.*, **13**, 054014.

Wilcox, B., Wilding, L., and Woodruff, C. (2007) Soil and topographic controls on runoff generation from stepped landforms in the Edwards Plateau of Central Texas. *Geophys. Res. Lett.*, **34**.

Wright, J. (1993) Nongrowing season ET from irrigated fields. [Allen, R. and Neale, C. (eds.)]. *Management of Irrigation and Drainage Systems: Integrated Perspectives,* ASCE Irrigation and Drainage Division, Park City, UT, 1005-1014.

Wuebbles, D., Fahey, K., Hibbard, D., Dokken, D., Stewart, D., and Maycock, T., Eds. (2017) *Climate Science Special Report*. Vol. I, *Fourth National Climate Assessment*, U.S. Global Change Research Program, 470 pp., https://doi.org/10.7930/J0J964J6.

Zhang, W., Villarini, G., Vecchi, G., Smith, J. (2018) Urbanization exacerbated the rainfall and flooding caused by hurricane Harvey in Houston. *Nature*, **563**, 384-388.

Zontarelli, L., Dukes, M., Romero, C., Migliaccio, K., and Morgan, K. (2010) Step by step calculation of the Penman-Monteith evapotranspiration (FAO-56 method). University of Florida Institute of Food and Agricultural Sciences Doc. AE459, 10 pp., https://edis.ifas.ufl.edu/ae459. Accessed 17 December 2020.